 CMES, vol.52, no.3, pp.217-235, 2009

Hydro-Mechanical Modelling of a Natural Slope Affected by a Multiple Slip Surface Failure Mechanism

A. Ferrari[1], **L. Laloui**[1,2] **and Ch. Bonnard**[1,3]

Abstract: A coupled hydro-mechanical formulation is presented for the analysis of landslide motion during crisis episodes. The mathematical formulation is used to model a natural slope affected by a multiple slip surface failure mechanism, in which pore water pressure evolution was identified as the main cause for movement accelerations. An elasto-plastic constitutive model is adopted for the behaviour of slip surfaces. Material parameters are obtained by combining the available laboratory tests and the back analysis of some crisis episodes. After being calibrated and validated, the model is applied to improve the understanding of the physical processes involved and to predict the landslide behaviour under different possible scenarios.

Keywords: landslide, hydro-mechanical coupling, multiple slip surfaces, unsaturated soil mechanics.

1 Introduction

Natural slopes in mountainous areas are often affected by slow-moving landslides of limited size. In particular in the Alpine arc, typical sliding areas present long term velocity between 1 and 10 cm/year. However, they may display occasional short term crises, generally as a consequence of exceptional climatic conditions, which can damage infrastructure assets and buildings. These situations represent a potential serious hazard that cannot be analysed in terms of probability analysis, as the number of recorded past events is generally very small and climate changes could significantly modify the environmental setting. Quantitative relationships relating climatic condition fluctuations and sliding area velocity must then be pursued by taking into account the most relevant physical processes involved in the landslide behaviours.

[1] Soil Mechanics Laboratory (LMS), Ecole Polytechnique Fédérale de Lausanne (EPFL), Switzerland.

[2] e-mail: lyesse.laloui@epfl.ch (corresponding author).

[3] Presently independent consultant, PBBG SA, Lausanne.

Conventional stability analyses are unable to deal with such questions because they do not allow the velocity fields to be determined. On the other hand, numerical modelling has been developed to predict landslide displacement patterns over time in order to deal with specific issues such as strain localisations and the development of shear zones [e.g. Dounias, Potts and Vaughan (1988); Troncone (2005)], viscous behaviours [e.g. Desai, Samtani and Vulliet (1995); Vulliet (2000)] and weathering processes [e.g. Eberhardt, Thuro and Luginbuehl (2005)]. This paper aims to describe the behaviour of slow-moving landslides by means of a coupled hydro-mechanical model. As is well known, the evolution of the pore water pressure within the landslide body is often recognized as the main cause for the occurrence of displacement accelerations. In this sense the interaction among the hydrological and the mechanical responses must be considered to analyse the landslide behaviour with the aim of quantitatively relating pore water pressure variations and movements.

Vertical displacement profiles of the horizontal displacements in slow-moving landslides often show that the deformation concentrates in thin layers while the rest of the landslide does not experience appreciable strains (Fig. 1). In a simplified attempt, the analysis of the landslide motion can then be tackled by considering the movement of masses with high rigidity sliding on deformable contact surfaces. Within the assumption of small displacements, the contacts among the various parts composing the landslide body can be modelled by means of continuum elements with proper constitutive laws.

In the following a coupled hydro-mechanical formulation is presented. A generalised effective stress is used to take into account the changes in the degree of saturation associated to the fluctuation of the groundwater level. An application is then presented for a real case, the Steinernase landslide (Switzerland) to demonstrate the adequacy and the usefulness of the proposed modelling approach.

2 Formulation of the hydro-mechanical coupling

When the failure mechanism of the slope is located above the piezometric line, it is likely that movement accelerations can occur as a consequence of the changes in the degree of saturation of the materials at the slip surface, due to the fluctuation of the groundwater level. In such a case, the transition from a partially saturated to a fully saturated state of the soil must be taken into account. An unsaturated soil is a three-phase medium composed of solid, liquid and gaseous phases. For the present case, an equivalent two-phase medium with a compressible liquid phase is considered, in which air bubbles are trapped within water. The solid grains are treated as incompressible. The interaction between the pore fluid pressure and the mechanical behaviour of the solid skeleton is obtained with a Biot-type mathemat-

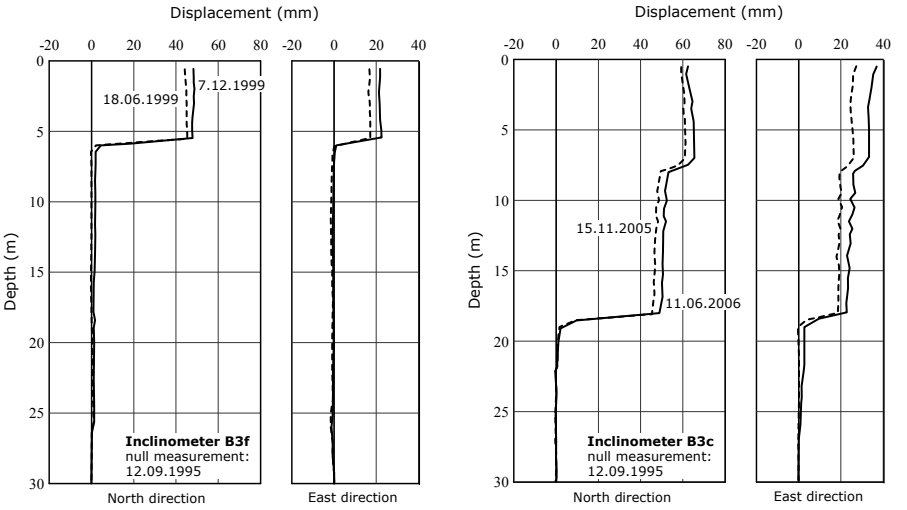

Figure 1: Example of inclinometer measurements for two different boreholes at the Steinernase landslide (Switzerland).

ical formulation [Biot (1956)], in which the mass and momentum of the fluid and solid phases are conserved. A thermodynamic description of the general form of the field equations is given in Laloui, Klubertanz and Vulliet (2003). The mass conservation equation of the soil is described by:

$$n\left(\beta_f S_r + \frac{dS_r}{dp}\right)\partial_t p + div\partial_t \mathbf{u}_{rf} + S_r\, div\partial_t \mathbf{u}_s = 0 \tag{1}$$

where p is the pore fluid pressure (compression pressure taken as positive), β_f is the compressibility of water, S_r is the degree of saturation and n is the porosity. The velocity vector of the fluid infiltration $\partial_t \mathbf{u}_{rf}$ links the absolute velocities of the fluid, $\partial_t \mathbf{u}_f$, and of the solid skeleton, $\partial_t \mathbf{u}_s$, by:

$$\partial_t \mathbf{u}_{rf} = n(\partial_t \mathbf{u}_f - \partial_t \mathbf{u}_s) \tag{2}$$

Darcy's law is then introduced to link the infiltration velocity with the hydraulic head:

$$\partial_t \mathbf{u}_{rf} = -\mathbf{K}^* \mathbf{grad}\,(p + \rho_f \mathbf{g}\mathbf{x}) \tag{3}$$

where ρ_f is the volumetric mass of the fluid, $\mathbf{g}$ is the vector of gravity acceleration, $\mathbf{x}$ is the position vector and $\mathbf{K}^*$ is the tensor of the kinematic soil permeability. In

unsaturated soils, $\mathbf{K}^*$ is a function of the degree of saturation S_r and is obtained by the multiplication of the tensor of the saturated permeability $\mathbf{K}$ by a scalar function, $k_r(S_r)$:

$$\mathbf{K}^* = k_r \mathbf{K} \tag{4}$$

The expression proposed by Van Genuchten (1980) is used:

$$k_r = \left(\frac{S_r - S_{r,res}}{1 - S_{r,res}} \right)^3 \tag{5}$$

where $S_{r,res}$ is the residual degree of saturation. Retention curves relate the degree of saturation to the pore fluid pressure. The following expression is used [Van Genuchten, (1980)]:

$$\begin{cases} S_r = S_{r,res} + \dfrac{1 - S_{r,res}}{\left[1 + \left(\alpha \dfrac{p}{\rho_f g} \right)^2 \right]^{1/2}} & \text{if } p < 0 \\ S_r = 1 & \text{if } p \geq 0 \end{cases} \tag{6}$$

where α is a material parameter. As a first approximation, hysteretical effects and retention behaviour dependency on density are neglected by assuming a constant value for α. Thus, the mass conservation is expressed by:

$$S_r div \partial_t \mathbf{u}_s = div \left[\mathbf{K}^* \mathbf{grad} \left(p + \rho_f \mathbf{gx} \right) \right] - n \left(\beta_f S_r + \frac{dS_r}{dp} \right) \partial_t p \tag{7}$$

which expresses how the temporal variation of the solid displacement (left side term) may be modified by the Darcy's flow (first right side term) and/or by the pore fluid pressure variation (second right term).

The soil equilibrium equation is given by:

$$div \boldsymbol{\sigma} - \rho \mathbf{g} = \mathbf{0} \tag{8}$$

where $\boldsymbol{\sigma}$ is the total (Cauchy) stress tensor with compression stresses taken as positive, and ρ is the total average mass density $\rho = \rho_d + n S_r \rho_f$, with ρ_d being the mass density of the solid skeleton. The behaviour of the solid matrix is assumed to be governed by the generalised Bishop's effective stress equation [Nuth and Laloui (2008); Laloui and Nuth (2009)] given by:

$$\boldsymbol{\sigma}' = \boldsymbol{\sigma} - S_r p \boldsymbol{\delta} \tag{9}$$

where $\boldsymbol{\sigma}'$ is the effective stress tensor, and $\boldsymbol{\delta}$ is the Kroenecker's delta. Eq. (9) ensures a smooth transition from the partial to the full saturation condition, providing the Terzaghi effective stress definition when S_r becomes equal to 1. The effective stress tensor may be expressed in terms of the constitutive tensor $\mathbf{C}$ and the total strain tensor $\boldsymbol{\varepsilon}$, defined as

$$\boldsymbol{\varepsilon} = \left(\nabla \mathbf{u}_s + (\nabla \mathbf{u}_s)^T\right)/2 \tag{10}$$

where the superscript T expresses the transposition of the tensor. The momentum conservation equation then takes the form:

$$div\{\mathbf{C} : \boldsymbol{\varepsilon}(\mathbf{u}_s)\} = \rho \mathbf{g} - S_r \mathbf{grad} p \tag{11}$$

Equations (7) and (11) comprise the two field equations with two unknowns $(\mathbf{u}_s, p)$.

Two different constitutive laws are considered: a non-deformable model (represented by an elastic model with high rigidities) for the soil not expected to experience appreciable deformations and a modified Cam-Clay elasto-plastic model [Roscoe and Burland (1968)] for the material at the slip surfaces. The use of continuum elements to simulate the relative displacements accumulating between the different slip surfaces is justified by taking into account the limited ranges of the measured displacements. The modified Cam-Clay model allows the consideration of the influence of the confinement stress and of the overconsolidation ratio on the soil behaviour [Schofield and Worth (1968)]. For the elasto-plastic model the strain rate $\dot{\boldsymbol{\varepsilon}}$ is assumed to be composed of two independent aliquots:

$$\dot{\boldsymbol{\varepsilon}} = \dot{\boldsymbol{\varepsilon}}_e + \dot{\boldsymbol{\varepsilon}}_p \tag{12}$$

The elastic strain rate $(\dot{\boldsymbol{\varepsilon}}_e)$ is obtained through the elastic stiffness tensor $(\mathbf{D})$ with the bulk modulus (K) and shear modulus (G) depending on the current stress level:

$$\dot{\boldsymbol{\varepsilon}}_e = \mathbf{D}^{-1} : \dot{\boldsymbol{\sigma}}' \tag{13}$$

$$K = \frac{(1+e_0)}{\kappa} p' \tag{14}$$

$$G = \frac{3}{2}\frac{1-2\nu}{1+\nu} K \tag{15}$$

where e_0 is the initial void ratio, p' is the mean effective stress, κ is the slope of the unloading-reloading lines in the $(\ln p', e)$ plane and ν is the Poisson's ratio.

Plastic strain increments $(\dot{\boldsymbol{\varepsilon}}_p)$ are produced when the stress state reaches the yield limit described by the following equation in the (p', q) plane:

$$f(p', q, p'_c) = q^2 - M^2 r^2 p'(p'_c - p') = 0 \tag{16}$$

where q is the deviatoric stress; M is the slope of the critical state line in the (p',q) plane; p'_c is the preconsolidation pressure, which controls the size of the yield locus; and r is a function of Lode's parameter θ, which enables the extension of the elliptic yield locus in the (p', q) plane in the principal stress space by a its rotation around the p' axis [Van Eekelen (1980)].

An associated plastic flow rule is assumed:

$$\dot{\boldsymbol{\varepsilon}}_p = \Lambda \frac{\partial f}{\partial \boldsymbol{\sigma}'} \tag{17}$$

where Λ is the plastic multiplier. A volumetric hardening relates the change in the size of the yield locus to the increment of the volumetric plastic strain ($\dot{\varepsilon}^v_p$):

$$\dot{p'}_c = -\frac{1+e_0}{\lambda-\kappa} p'_c \dot{\varepsilon}^v_p \tag{18}$$

3 Main features of the landslide

The Steinernase landslide was identified on the bank of the Rhine between the towns of Stein and Mumpf in the canton of Aargau in Switzerland. It covers an area of some 7 ha. Three infrastructure assets are located at the slope toe, namely a railway, a highway and a cantonal road connecting Zurich and Basel. The presence of a slide had been known for many years, and the slope has been monitored since 1986, with data collection on movements and pore water pressures in the area. It has been difficult for the authorities to determine if the slide might be liable to experience a serious crisis, under what conditions (maybe related to climate change) and what the consecutive displacements would be.

A general plan of the slope is depicted in Fig. 2, showing the locations where displacement data were collected. The figure also shows the active zone, which extends from the mountain road to the railway, approximately 300 m in width and 230 m in length. Evidence of superficial instabilities led to the conclusion that this active zone is part of a wider substable zone that extends longitudinally from the beginning of the slope main scarp to the cantonal road.

Readings pointed out that the displacements are directed towards the slope fall line (Fig. 2). Moreover, inclinometer profiles clearly show the presence of a multiple surface failure mechanism: a unique slip surface, present in the upper part of the slope, develops into a multi-surface system in the toe zone. Up to three distinct failure surfaces were observed in the same vertical profile (in inclinometer B3d). As an example, data on displacements over time from inclinometer B3c for two different depths are plotted in Fig. 3. The plot indicates that during crisis episodes, the more

superficial part of the landslide body undergoes noticeable relative movement with respect to the deeper part and a relative displacement accumulates.

Pore water pressure variation within the slope was recognized as the main cause for accelerations. The trend of the total head recorded at 10 m depth is also plotted in Fig. 3 for borehole B3c. Inclinometer reading delays do not allow us to assess the exact instants in which movements start and end; however, it is worthwhile to note that sudden displacement increases coincided with total head peaks. The groundwater table does not seem to reach the topographic surface. Even during more intense increases in pore water pressure, the free surface seems to reach the level of the most superficial sliding surface.

The general trends of displacement data suggest that some creep effect is also taking place. A creep velocity of about 2 mm/year on an average has been estimated, based on long-term monitoring data. However, this effect is considered of secondary importance when compared to the displacement accumulations induced by the pore water pressure fluctuations.

A schematic of the multi-surface system is shown in Fig. 4, in which a cross-section along the centre of the active zone is reported (profile A-A' in Fig. 2). Even if no displacement measurements have been performed in the toe of the landslide and a detailed position of the sliding surface cannot be identified in that zone, it appears that the deep-seated sliding surface (related to the substable area) reaches the slope between the cantonal road and the highway. In this sense, dangers for the infrastructures would be most related to a possible reactivation of deep movements.

Three main materials have been identified from the analysis of the boreholes, and they are indicated in the figure: (i) the soil cover, (ii) the bedrock and (iii) the Rhine alluvium. In spite of some heterogeneity in index properties at a local scale, the soil of the landslide body is homogeneous at the scale of the landslide, and it was classified as CL.

4 The finite element model

The challenge in this present case, affected by minor crises of 1 to 2 cm in winter, was to verify if the proposed model would be precise enough to reproduce the observed crisis episodes and then to allow the quantification of expected displacements in modified conditions, like exceptional rainfall events or the construction of a drainage scheme aimed at protecting the main highway and the main railway line between Basel and Zurich.

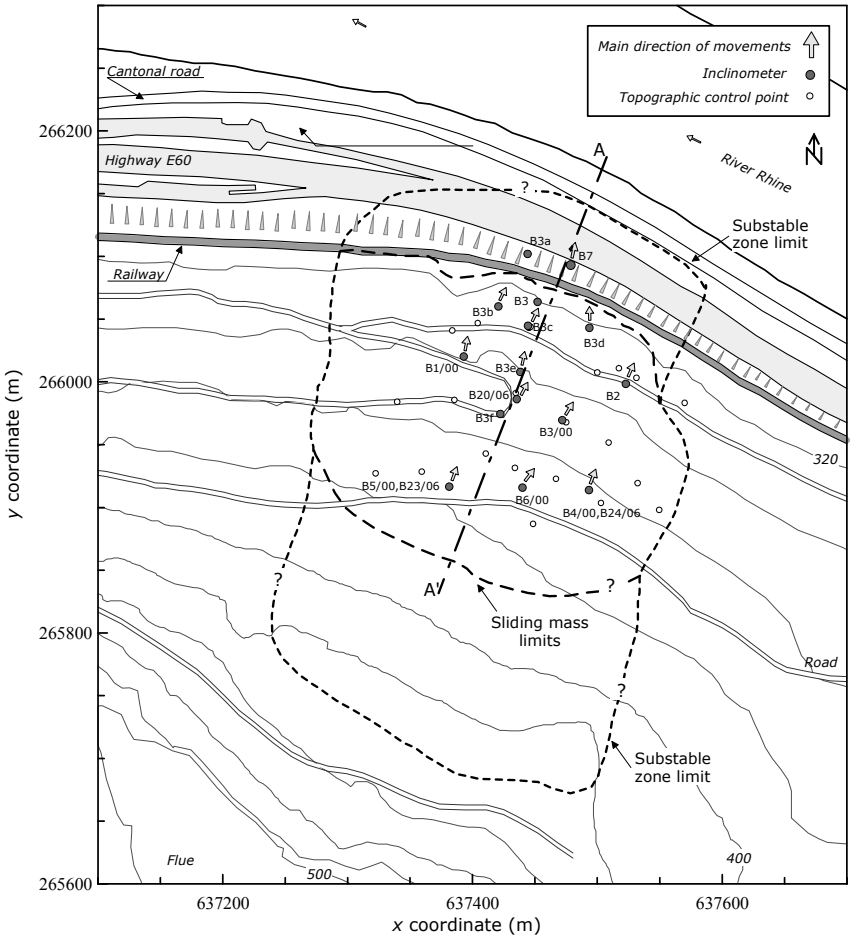

Figure 2: The Steinernase landslide: general plan showing the position of inclinometers and topographic control points. Limits of the active and substable zones and main direction of movements are shown.

4.1 Mesh and boundary conditions

The two-dimensional mesh used for the model was created on the cross-section passing through the centre of the landslide. The unstructured mesh includes 1694 nodes and 1554 isoparametric 4-node elements (Fig. 5). The presence of relative displacements within the landslide was considered an important feature to be explicitly taken into account in the model. For this reason, three independent slip surfaces were introduced, allowing the selection of different constitutive parameters

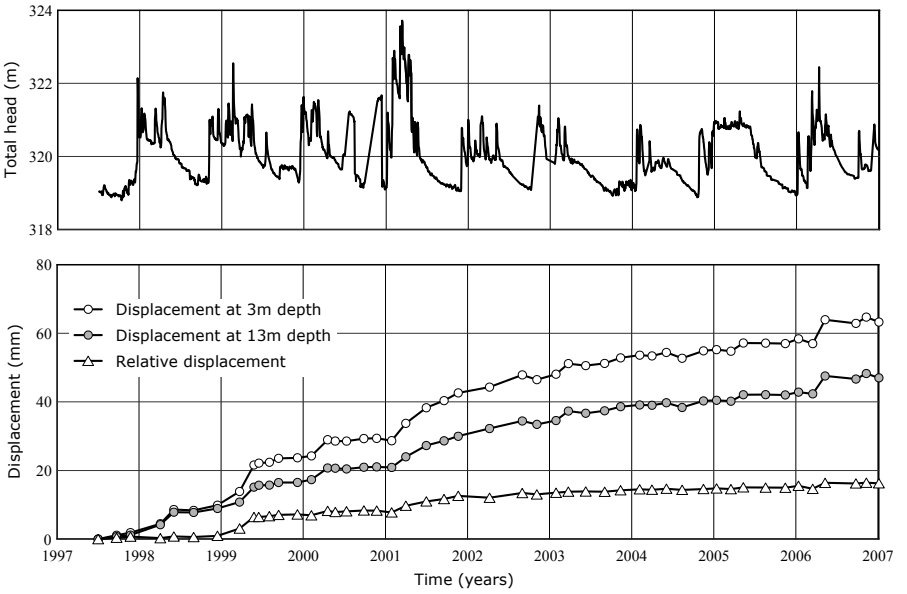

Figure 3: Total head at 10m depth and displacements at two different depths registered at borehole B3c.

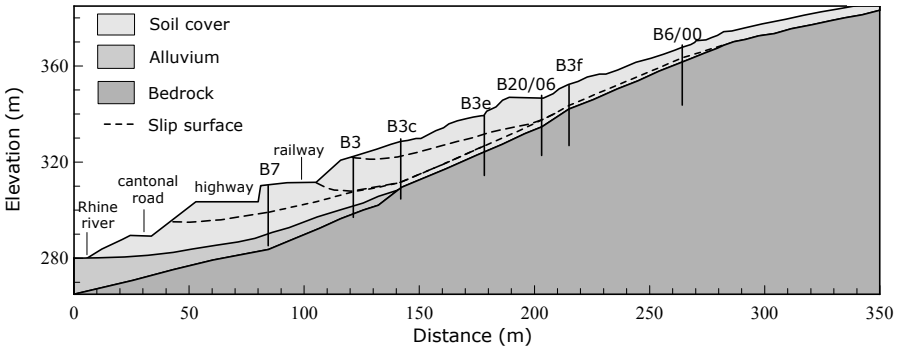

Figure 4: Cross-section along the centre of the landslide, indicating the multiple slip surface system as interpreted from inclinometer readings.

for each of them; their positions were carefully reconstructed taking into account the inclinometer profiles for the instrumented boreholes close to the cross-section.

As suggested by the inclinometer indications, fixed nodes were assumed at the bottom of the domain for the deepest layers of alluvium and bedrock. Only horizontal

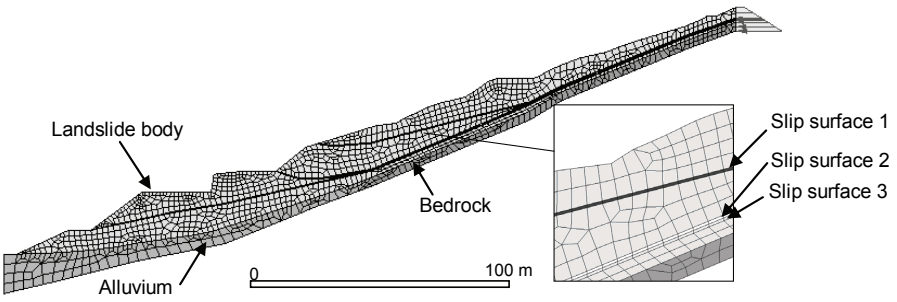

Figure 5: Finite element mesh for the hydro-mechanical model.

displacements were prevented for the bedrock nodes of the left edge. Equivalent loading forces were applied at the right edge of the mesh. A specific parametric study was performed, testing different lateral stress distributions on the edge. As a result it was clear that this boundary condition did not play a fundamental role for the general pattern of displacements, and an active state was assumed. The initial state of stress is that induced by the soil weight at rest. This assumption is corroborated by the normal consolidated condition of the soils within the slope, pointed out by the available oedometric tests.

As for the hydraulic boundary conditions, because pore water pressure variations were identified as the main cause for soil mass accelerations, an extensive analysis of the hydro-geological features of the slope was performed by the Laboratory of Engineering and Environmental Geology (GEOLEP) at the EPFL [EPFL (2008)]. This study pointed out the role of several key factors on the evolution of pore water pressure within the slope, such as infiltration, preferential flows and vegetation. A 3D finite element hydrological model was calibrated and validated in order to predict the pore water pressure evolution in the area of interest for the years 2000, 2001 and 2006. As an example, Fig. 6 shows the comparison between the measured and the computed total head at borehole B3c at a 10 m depth for the years 2000 and 2001. Computed groundwater pressures resulting from the hydro-geological simulation were introduced as nodal forces in the hydro-mechanical model, in a similar manner as performed by François, Tacher, Bonnard, Laloui and Triguero (2007). They varied over time at selected nodes of the model. Special elements (*seepage elements*) were introduced for the superior edges of the domain. These elements prevent the increase of compressive pore water pressure values in the nodes at the topographic surface, allowing simulation of the superficial runoff of the infiltrating rain when the superficial layers become fully saturated. In this case,

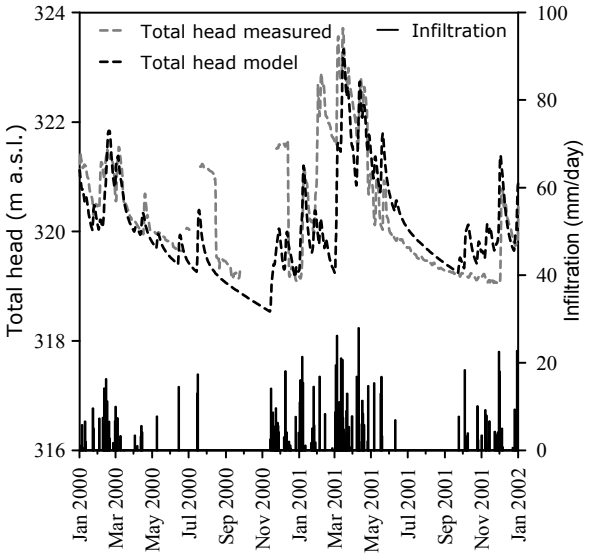

Figure 6: Comparison of measured and computed total head by the hydro-geological model for the calibration period 2000-2001 (after [GEOLEP/EPFL (2008)]).

a zero pore water pressure value is automatically imposed in these nodes in order to avoid unrealistic compressive pore water pressure values for the nodes at the topographic surface.

The finite element geomechanical calculation was carried out with the Z_SOIL® code, which includes the mathematical hydro-mechanical formulation as well as the constitutive law presented in the previous section.

4.2 Calibration and validation of the model

The model was calibrated for the period between 1 January, 2000 and 31 December, 2001, during which two acceleration phases were detected (Fig. 3). Material parameters were chosen, taking into account the indications coming from laboratory tests results [Geotest (1997)]. Suitable values were selected to represent the behaviour of the materials at the scale of the landslide. These values are reported in Table 1, where E' is the Young modulus, ν' is the Poisson's ratio, λ and κ are the slopes of the virgin consolidation line and of the swelling line, respectively, M is the slope of the critical state line and γ is the unit volume weight. The model proposed by Arya and Paris (1981) was used, providing information on the retention

behaviour of the soil based on the knowledge of grain size distributions and density. The analysis resulted in $\alpha = 1\ m^{-1}$ in Eq. 6, corresponding to an air entry value of approximately 10 kPa, in accordance with the presence of a wide sand fraction in the grain size distribution.

As a result of the calibration, the model reproduced the observed displacement patterns through the entire domain for the considered period well (Fig. 7): larger displacements were correctly predicted for the upper part of the landslide body.

To evaluate the adequacy of the model assumptions for the materials at the slip surfaces, Fig. 8 depicts the inclinometer profile at the borehole B3e obtained from the simulation. The comparison with the measured inclinometer shape allows concluding that the strain concentration at the slip surfaces is well reproduced, considering the precision of inclinometer data.

For a quantitative assessment of the model capabilities, Fig. 9 shows observed and computed displacements for borehole B3e at two different depths, namely 3 and 9 m. The plot shows that accelerations that occurred during crisis periods are reproduced well, both in terms of durations and accumulated displacements. In accordance with measurements in the field, larger displacements are computed for the more superficial part of the slope. Higher displacement values with respect to the measured ones are predicted for the borehole B3e at 3m during the second acceleration phase. This result is in accordance with the fact that the installed inclinometer in that borehole was sheared during that event.

Computed pore water pressures for the same nodes are also represented in Fig. 9 (positive values refer to compressions). The plots allow the appreciation of the quantitative correlation between the evolution of displacement and the evolution of pore water pressure, which constitutes the key point of the coupled hydro-mechanical model. These plots also indicate that displacements in the more superficial part of the slope can be initiated by a reduction (in absolute value) of the negative pore water pressure (suction).

Once the model was calibrated, its prediction capabilities were assessed for the year 2006. Pore water pressure evolution for each mesh node was obtained by the validation of the hydrogeological model. Comparison between predicted and measured displacements at borehole B3c is reported in Fig. 10. In general, a quite satisfactory agreement was observed (in the millimetre range).

4.3 Model response to different scenarios

The prediction capabilities of the model have been used in order to simulate the behaviour of the slope when subjected to pore water pressure distributions induced by different rainfall patterns and to assess possible stabilisation strategies. As an

Table 1: Constitutive parameters.

MATERIAL	Landslide body	Alluvium	Bedrock	Sliding surface 1	Sliding surface 2	Sliding surface 3
Constitutive law	Elastic	Elastic	Elastic	Modified Cam Clay	Modified Cam Clay	Modified Cam Clay
E' (kPa)	60'000	200'000	500'000	-	-	-
ν'	0.3	0.3	0.3	0.3	0.3	0.3
λ	-	-	-	0.1	0.1	0.1
κ	-	-	-	0.05	0.05	0.05
M	-	-	-	0.90	0.95	1.00
γ(kN/m^3)	17	17	25	17	17	17

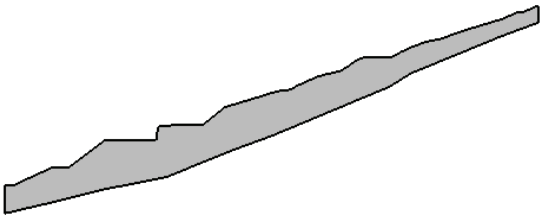

1/01/2000, day 0, reference date for displacement computation.

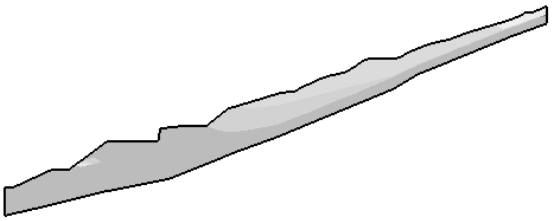

1/03/2000, day 60, accumulated horizontal displacements at the end of the first considered acceleration phase.

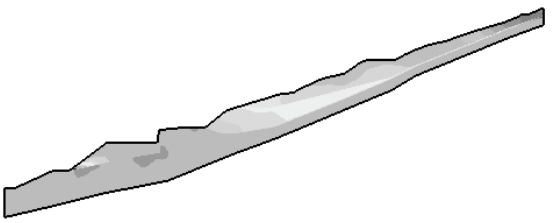

18/04/2001, day 473, accumulated horizontal displacements at the end of the second considered acceleration phase.

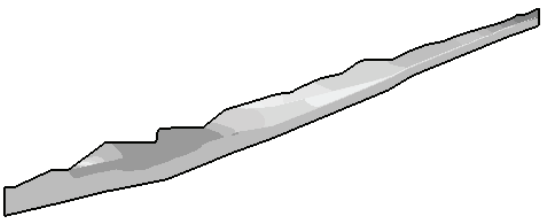

31/12/2001, day 730, accumulated horizontal displacements at the end of the 2 years considered in the calibration phase.

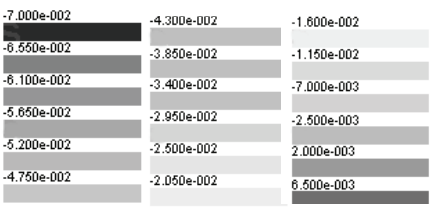

Figure 7: Computed horizontal displacement patterns (in m) at different times (negative sign refers to downhill displacements).

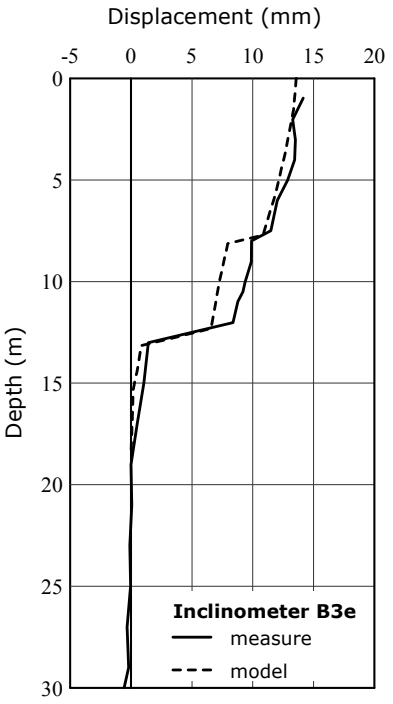

Figure 8: Comparison between the computed and the measured inclinometer profiles at the borehole B3e for the period 23/5/2000 – 2/4/2001.

example of the first case, pore water pressure distributions for the period 2000-2001 provided by the hydro-geological model were incremented by 10% in order to simulate, as a first approximation, an increase in the total amount of rainfall, without a significant change in rainfall pattern. Horizontal displacements for borehole B3e at 3 m of depth are reported in Fig. 11. The comparison with the displacement at the same point associated with the original pore water pressure distribution indicates an almost linear increase of 10% in the final cumulated displacement. It seems, therefore, that a constant and diffused increase (with small amplitude) of the pore water pressure distribution within the slope will not significantly change the overall landslide response, affecting only the final cumulative displacement.

As an example of the model application to assess stabilisation strategy efficiency, displacement trends for year 2000-2001 were predicted for the case in which a system of sub-horizontal drains at the slope toe was installed. This analysis considered 50 m long drains drilled from the cantonal road. The presence of the drains was introduced as a boundary condition in the hydro-geological model, and a new

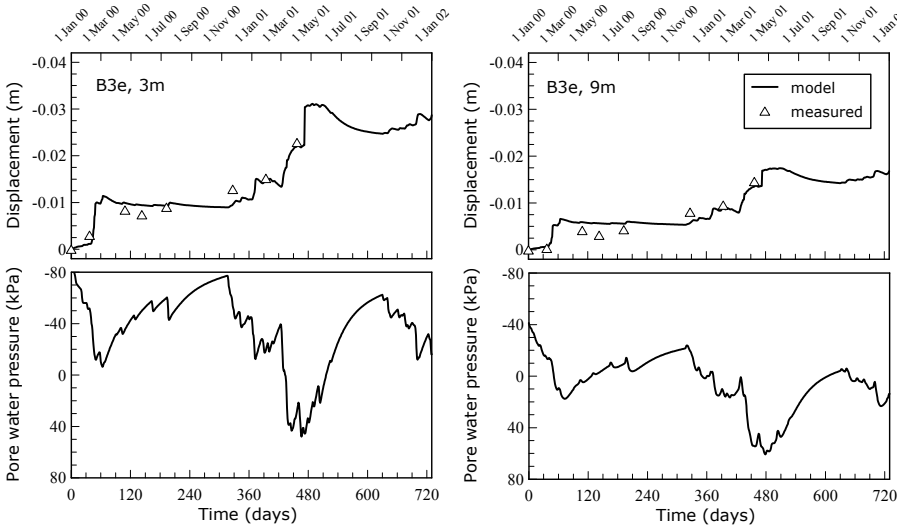

Figure 9: Computed and measured horizontal displacements and evolution of the computed pore water pressures at borehole B3e for the period 1/01/2000-31/12/2001 (negative sign refers to downhill displacements).

distribution of pore water pressure was obtained for the period in question. Predicted displacements are reported in Fig. 12 for borehole B3e at different depths. Comparison with the original scenario shows that the drainage system, even if realized at the slope toe, would have a positive effect in terms of movement reduction, including the upper part of the slope.

5 Conclusions

The coupled hydro-mechanical model presented reproduced the behaviour of the landslide considered in this study quite well. Specific features of the problem such as the presence of the multiple slip surface system and the coupling between pore water pressure evolution and movements were tackled with advanced finite element modelling. The agreement between measured and predicted displacements was good.

The model sheds light on the physical processes involved in the landslide; in particular, it appears that the transition from partial to full saturation plays a major role in the accelerations in the movement of the superficial material in the landslide, even though the total displacements are quite small.

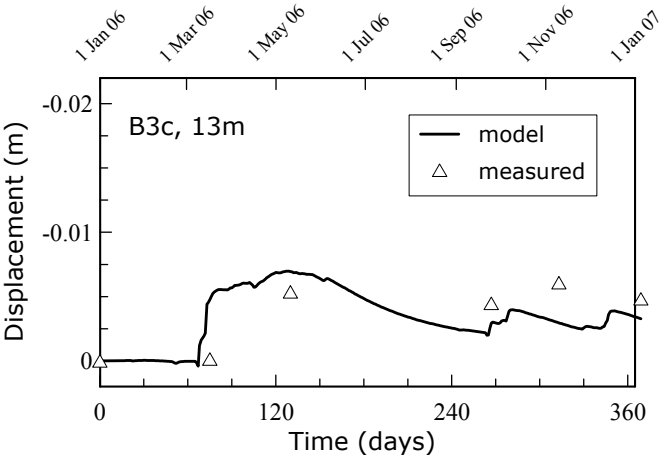

Figure 10: Predicted and measured horizontal displacements at borehole B3c for the year 2006.

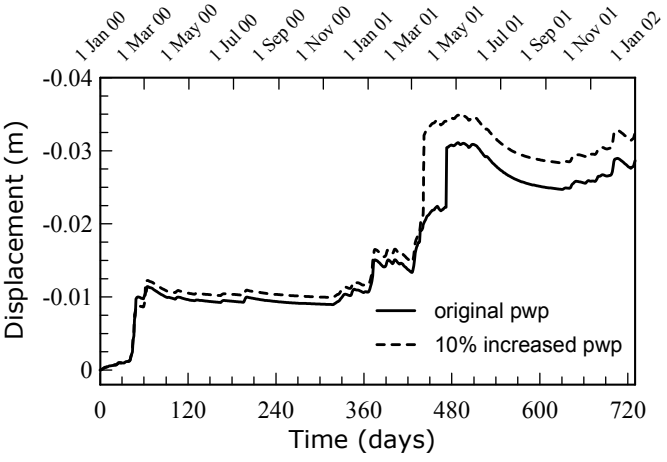

Figure 11: Predicted horizontal displacements for a 10% pore water pressure (pwp) increase at borehole B3e at 3m of depth.

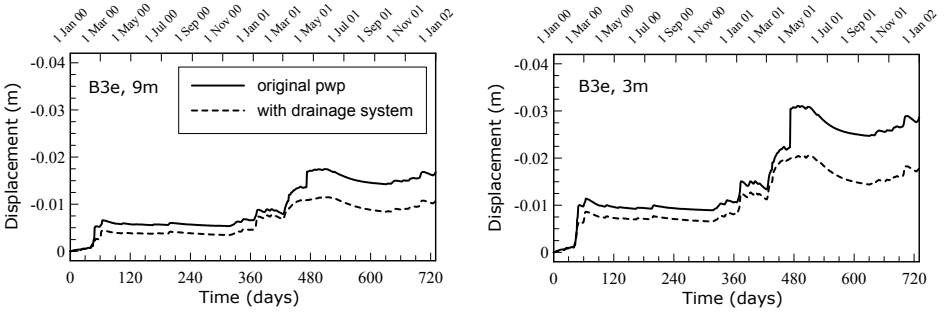

Figure 12: Predicted horizontal displacements at borehole B3e for the scenario with sub-horizontal drains.

The analysis of the multiple slip surface mechanism showed that the infrastructure at the toe of the landslide is most directly affected by the deepest slip surface, despite the fact that the movements at the deepest surface were of very low intensities during the measurement campaign (1995-2007). These dangers may be mitigated by drainage at the toe.

Acknowledgement: The authors express their thanks for the support provided by the Swiss Federal Road Office for this fascinating research. They also wish to acknowledge the Laboratory of Engineering and Environmental Geology (GEOLEP) at the EPFL for the development of the hydro-geological model. Their thanks are also addressed to Dr. Peter Kleboth (GEOTEST AG) for providing field data. The first author wishes to acknowledge the support of the European Community under the Marie Curie Research Training Network "Mountain Risks: from prediction to management and governance".

References

Arya, L. M.; Paris, J. F. (1981): A physicoempirical model to predict soil moisture characteristics from particle-size distribution and bulk density data. *Soil Sci. Soc. Am. J.* vol. 45, pp. 1023–1030.

Biot, M. A. (1956): General solution of the equations of elasticity and consolidation for a porous material. *Journal of Applied Mechanics*, vol. 19, pp. 91-96.

Desai, C. S.; Samtani, N. C.; Vulliet, L. (1995): Constitutive modelling and analyses of creeping slopes. *Journal of Geotechnical Engineering*, ASCE, vol. 121(1), pp. 155-75.

Dounias, G. T.; Potts, D. M.; Vaughan, P. R. (1988): Finite element analyses

of progressive failure: two case studies. *Computers and Geotechnics*, vol. 6, pp. 155-175.

Eberhardt, E.; Thuro, K.; Luginbuehl, M. (2005): Slope instability mechanisms in dipping interbedded conglomerates and weathered marls—the 1999 Rufi landslide, Switzerland. *Engineering Geology*, vol. **77**(1), pp. 35-56.

EPFL (2008): Geologische, hydrogeologische (GEOLEP) und geomechanische (LMS) Modellierung des Erdrutsches bei Stein-Mumpf (AG). Schlussbericht. Ecole Polytechnique Fédérale de Lausanne, Switzerland.

François, B.; Tacher L.; Bonnard Ch.; Laloui L.; Triguero V. (2007): Numerical modelling of the hydrogeological and geomechanical behaviour of a large slope movement: The Triesenberg landslide (Liechtenstein), *Canadian Geotechnical Journal*, vol. 44, pp. 840-857.

Geotest AG (1997): Prüfbericht Labor Nr. Z9608.430.

Laloui, L.; Klubertanz, G.; Vulliet, L. (2003): Solid-liquid-air coupling in multiphase porous media. *International Journal of Numerical and Analytical Methods in Geomechanics*, vol. 27(3), pp. 183-206.

Laloui, L.; Nuth, M. (2009): On the use of the generalised effective stress in the constitutive modelling of unsaturated soils. *Computer and Geotechnics*, Vol. 36 (1-2): 20-23.

Nuth M.; Laloui L. (2008): Effective Stress Concept in Unsaturated Soils: Clarification and Validation of a Unified Framework. *International Journal of Numerical and Analytical Methods in Geomechanics*, vol. 32, pp. 771-801.

Roscoe, K. H; and Burland, J. B. (1968): On the generalized stress–strain behaviour of "wet" clay. In: Engineering plasticity. Edited by J. Heyman and F.A. Leckie. Cambridge University Press, Cambridge, England, pp. 535–609.

Schofield, A.; Worth, P. (1968): Critical state soil mechanics. McGraw-Hill, London.

Troncone, A. (2005): Numerical analysis of a landslide in soils with strain-softening behaviour. Géotechnique, vol. 55(8), pp. 585–596.

Van Eekelen, H. A. M. (1980): Isotropic yield surfaces in three dimensions for use in soil mechanics. *International Journal of Numerical and Analytical Methods in Geomechanics,* vol. 4, pp. 89–101.

Van Genuchten, M. T. (1980): A closed form equation for predicting the hydraulic conductivity of unsaturated soils. *Soil Sci. Soc. Am. J.*, vol. 44, pp. 892–898.

Vulliet, L. (2000): Natural slopes in slow movement. In Modeling in geomechanics. Edited by M. Zaman, G. Gioda, and J. Booker. John Wiley, Chichester, U.K.